

HYDROGEN-POOR SUPERLUMINOUS SUPERNOVAE WITH LATE-TIME H α EMISSION: THREE EVENTS FROM THE INTERMEDIATE PALOMAR TRANSIENT FACTORY

LIN YAN^{1,2}, R. LUNNAN³, D. A. PERLEY^{4,5}, A. GAL-YAM⁶, O. YARON⁶, R. ROY⁷, R. QUIMBY^{8,9}, J. SOLLERMAN⁷, C. FREMLING⁷, G. LELOUDAS^{4,6}, S. B. CENKO^{10,11}, P. VREESWIJK⁶, A. DE CIA^{6,12}, E. O. OFEK⁶, S. R. KULKARNI^{2,3}, F. MASCI¹, U. D. REBBAPRAGADA¹³, P. WOŹNIAK¹⁴

To be submitted to the Astrophysical Journal

ABSTRACT

We present observations of two new hydrogen-poor superluminous supernovae (SLSN-I), iPTF15esb and iPTF16bad, showing late-time H α emission. Including the previously published iPTF13ehe, this makes up a total of three such events to date. iPTF13ehe is one of the most luminous and the slowest evolving SLSNe-I, whereas the other two are less luminous and fast decliners. The H α lines are as luminous as $(1 - 3) \times 10^{41}$ erg s⁻¹ with FWHM widths of (4000-6000) km s⁻¹. We interpret this as a result of the ejecta running into a neutral H-shell located at a radius of several times 10¹⁶ cm. This implies that an episode of violent mass loss must have occurred several decades before the supernova explosion. Such a short time interval suggests that eruptive mass loss could be common prior to the death of a massive star as a SLSN. This also implies that helium is unlikely to be completely stripped off the progenitor stars and could be present in the ejecta. It is a mystery why helium features are not detected, even though non-thermal energy sources, capable of ionizing He atoms, may exist as suggested by the O II absorption series in the early time spectra. At late times (+240 d), our spectra appear to have intrinsically lower [O I] 6300 Å luminosities than that of SN2015bn and SN2007bi, possibly an indication of smaller oxygen masses ($< 10 - 30 M_{\odot}$). In addition, for all three events, the broad H α lines are initially blue-shifted relative to the host galaxies. This result is in tension with the binary star model proposed for iPTF13ehe. Finally, iPTF15esb has a peculiar LC with semi-periodic undulations with a time scale of 22 days, and higher amplitudes in bluer bands. One possible explanation is ejecta-CSM interaction. Together with late-time H α emission, these observations imply the presence of both H-poor and H-rich CSM shells in iPTF15esb.

Subject headings: Stars: supernova, massive stars

1. INTRODUCTION

Superluminous supernovae (SLSNe; Gal-Yam 2012) are rare stellar explosions, radiating 10 – 100 times more

¹ MS100-22, Caltech/IPAC, California Institute of Technology, Pasadena, CA 91125, lyan@caltech.edu

² Caltech Optical Observatories, California Institute of Technology, Pasadena, CA 91125

³ Department of Astronomy, California Institute of Technology, 1200 East California Boulevard, Pasadena, CA 91125

⁴ Dark Cosmology Centre, Niels Bohr Institute, University of Copenhagen, Juliane Maries Vej 30, DK-2100, Copenhagen, Denmark

⁵ Astrophysics Research Institute, Liverpool John Moores University, IC2, Liverpool Science Park, 146 Brownlow Hill, Liverpool L3 5RF, UK

⁶ Benoziyo Center for Astrophysics and the Helen Kimmel Center for Planetary Science, Weizmann Institute of Science, 76100 Rehovot, Israel

⁷ The Oskar Klein Centre, Department of Astronomy, Stockholm University, AlbaNova, 10691, Stockholm, Sweden

⁸ Department of Astronomy, San Diego State University, San Diego, CA 92182, USA

⁹ Kavli IPMU (WPI), UTIAS, The University of Tokyo, Kashiwa, Chiba 277-8583, Japan

¹⁰ Astrophysics Science Division, NASA Goddard Space Flight Center, Mail Code 661, Greenbelt, MD 20771, USA

¹¹ Joint Space-Science Institute, University of Maryland, College Park, MD 20742, USA

¹² European Southern Observatory, Karl-Schwarzschild-Strasse 2, 85748 Garching bei München, Germany

¹³ Jet Propulsion Laboratory, California Institute of Technology, Pasadena, CA 91109, USA

¹⁴ Space and Remote Sensing, ISR-2, MS-B244 Los Alamos National Laboratory, Los Alamos, NM 87545, USA

energy than normal supernovae. Their extreme peak luminosities and slowly evolving light curves (LC) cannot be explained by standard models based on radioactive decay of ⁵⁶Ni. Although the detailed physics of SLSNe is not understood, a general consensus from published studies is that their progenitors are massive stars, $> 30 - 100 M_{\odot}$ (Quimby et al. 2011; Gal-Yam et al. 2009; Smith et al. 2007; Ofek et al. 2007; Nicholl et al. 2014; Yan et al. 2015). Observations of SLSNe have highlighted our poor understanding of the late stages of massive star evolution, especially mass loss processes. According to standard stellar evolutionary models, massive stars ($> 30 M_{\odot}$) are thought to have very little hydrogen at the time of supernova explosion (Georgy et al. 2012; Smith 2014; Langer 2012). However, detections of two types of SLSNe – one with and one without H and He (SLSN-II and SLSN-I respectively, Gal-Yam et al. 2012) – illustrate a much more complex picture of massive star evolution, and indicate that their massive progenitors must have two distinctly different mass loss histories. Progenitors of SLSN-I lose their H-envelope long before core explosion. In contrast, for a progenitor of a SLSN-II, the stripping of its H-envelope must be incomplete, and the bulk of the H-rich medium is still either loosely bound to or very close to the progenitor at the time of the supernova explosion.

If the observational appearance of a SLSN is largely affected by its progenitor mass loss history, one could imagine if there may be SLSNe-II whose progenitors have

retained a small amount of H or SLSNe-I whose progenitors lost all of the H-envelope only shortly before the supernova explosion. The former events would not have characteristics of SNe IIn, with both narrow and broad $H\alpha$ emission, indicating ejecta interaction with extended, dense H-rich circumstellar medium (CSM). This type of transient may have been detected already, for example, SN 2008es, SN 2013hx, PS15br and possibly CSS121015 (Miller et al. 2009; Gezari et al. 2009; Benetti et al. 2014; Inserra et al. 2016a), which show only broad $H\alpha$ emission in the photospheric phase. In the latter case of stars losing their H-envelope shortly prior to explosion, the H-rich material would not have enough time to be completely dispersed into the interstellar medium (ISM) and would be located close enough so that when the supernova explodes, the SN ejecta would be able to catch up with this H-shell, and the subsequent interaction would produce broad $H\alpha$ emission in late-time spectra. Our observation of SLSN-I iPTF13ehe suggests that indeed such events exist (Yan et al. 2015).

Systematic follow-up observations have led to discoveries of new features from SLSNe-I, including double peak LCs at early times (Nicholl et al. 2015; Vreeswijk et al. 2017; Smith et al. 2016), and broad $H\alpha$ and [O III] 4363 & 5007Å emission in late-time spectra of SLSNe-I (Yan et al. 2015; Lunnan et al. 2016). Well sampled light curves of SN 2015bn and iPTF13dcc have also resulted in discoveries of LC undulations of SLSNe-I, suggesting possible ejecta interaction with H-poor CSM (Nicholl et al. 2016; Vreeswijk et al. 2017).

In this paper, we report two new SLSNe-I events, iPTF15esb and iPTF16bad, showing late-time $H\alpha$ emission, similar to iPTF13ehe. In addition, the LC of iPTF15esb shows strong, semi-periodic undulations. This paper reports the new observations and presents a coherent analysis of all three events. We also discuss the implication for various physical models and the whole SLSN-I population. Throughout the paper, we adopt a Λ CDM cosmological model with $\Omega_M = 0.286$, $\Omega_\Lambda = 0.714$, and $H_0 = 69.6 \text{ kms}^{-1} \text{ Mpc}^{-1}$ (Planck Collaboration et al. 2016).

2. TARGETS AND OBSERVATIONS

We discuss a sample with three SLSNe-I discovered by the Intermediate Palomar Transient Factory (iPTF), including two new events (iPTF15esb and iPTF16bad) and one already published event (iPTF13ehe; Yan et al. 2015). The basic properties and the coordinates are summarized in Table 2. These three events are at a similar distance, $z \sim 0.224 - 0.3434$, the median redshift of PTF SLSNe, due to the survey sensitivity limit.

All three events have the identical Galactic extinction of $E(B - V) = 0.04$ magnitude (Schlafly & Finkbeiner 2011). All fluxes are corrected assuming the extinction law of Cardelli et al. (1989) with $R_V = A_V / E(B - V) = 3.1$. The host galaxies have either pre-explosion photometry from SDSS or measurements after the supernova has faded in the case of iPTF13ehe. The host of iPTF16bad is the faintest of the three, and is below the detection thresholds of SDSS in all filters. The hosts are low mass and star forming, typical of SLSN-I host galaxies as found by Lunnan et al. (2014), Leloudas et al. (2015), and Perley et al. (2016).

Photometric observations of iPTF15esb and

iPTF16bad were obtained with the Palomar 48 & 60 inch (P48 & P60), the 4.3 meter Discovery Channel Telescope (DCT) and the Las Cumbres Observatory Global Telescope Network (LCOGT). All reported photometry in Table 3 and 4 is in AB magnitudes and calibrated to the SDSS g, r, i filters. The P60 and LCOGT photometry is measured using a custom image subtraction software (Fremming et al. 2016) and the P48 using the PTF Image Differencing Extraction (PTFIDE) software (Masci et al. 2016).

iPTF15esb and iPTF16bad have spectra at 12 and 4 epochs, covering the rest-frame phase (relative to the peak date) from +0 to +320 and +3 to +242 days respectively (Table 1). These data were taken with the Double Beam SPectrograph (DBSP; Oke & Gunn 1982) on the 200 inch telescope at Palomar Observatory (P200), the Low-Resolution Imaging Spectrometer (LRIS; Oke et al. 1995) and the DEep Imaging Multi-Object Spectrograph (DEIMOS; Faber et al. 2003) on the Keck telescopes. The absolute flux calibration of these spectra is calibrated using the broad band photometry at the corresponding phase.

3. ANALYSIS AND RESULTS

3.1. Emergence of $H\alpha$ emission from H-poor SLSNe

The main result of this paper is the detection of broad $H\alpha$ emission in the late-time spectra of the three H-poor SLSNe. Figure 1 displays all of the available spectra for these three events, except two spectra of iPTF15esb at +270 and 320 days, which show only features from the host galaxy. In this figure, the spectra have not been host subtracted. It is apparent that broad $H\alpha$ emission lines start to emerge at late-times between photospheric and nebular phases. And they persist until fairly late-times, +123, +242 and 251 days for iPTF15esb, iPTF16bad and iPTF13ehe respectively, as shown in Figure 2. It is worth noting here that the LCs of iPTF15esb and iPTF16bad decline ~ 3 times faster than that of iPTF13ehe (see §3.2 for details). Therefore, the last spectrum from iPTF15esb at +123 d could be at a similar late phase as that of iPTF13ehe. In addition, Figure 2 compares our late-time spectra with the spectrum of SLSN-I SN2015bn (Nicholl et al. 2016), showing prominent broad $H\alpha$ emission and apparent weak [O I] 6300 Å lines from our three events. Quantitative discussion on [O I] 6300 Å is included in §4.

One important constraint is when $H\alpha$ is first detected in the available spectra. The answer affects how we calculate the distance the ejecta have traveled since the explosion. We display all of the available spectra for these three events in Figure 1. All spectroscopic data are listed in Table 1, and will be made available via WISeREP (Yaron & Gal-Yam 2012). For comparison, we also include the high SNR spectrum of Gaia16apd, which is the second closest SLSN-I ever discovered (Yan et al. 2016).

It is clear from Figure 1 that the answer to the above question is not obvious because before a spectrum becomes fully nebular, broad absorption features can make it difficult to determine where the true continuum is. For examples, does the +52 d spectrum for iPTF15esb (Figure 1) have $H\alpha$ emission? And is the broad bump near 6500Å in the +0d day spectrum of iPTF16bad $H\alpha$, or continuum between two broad absorption features?

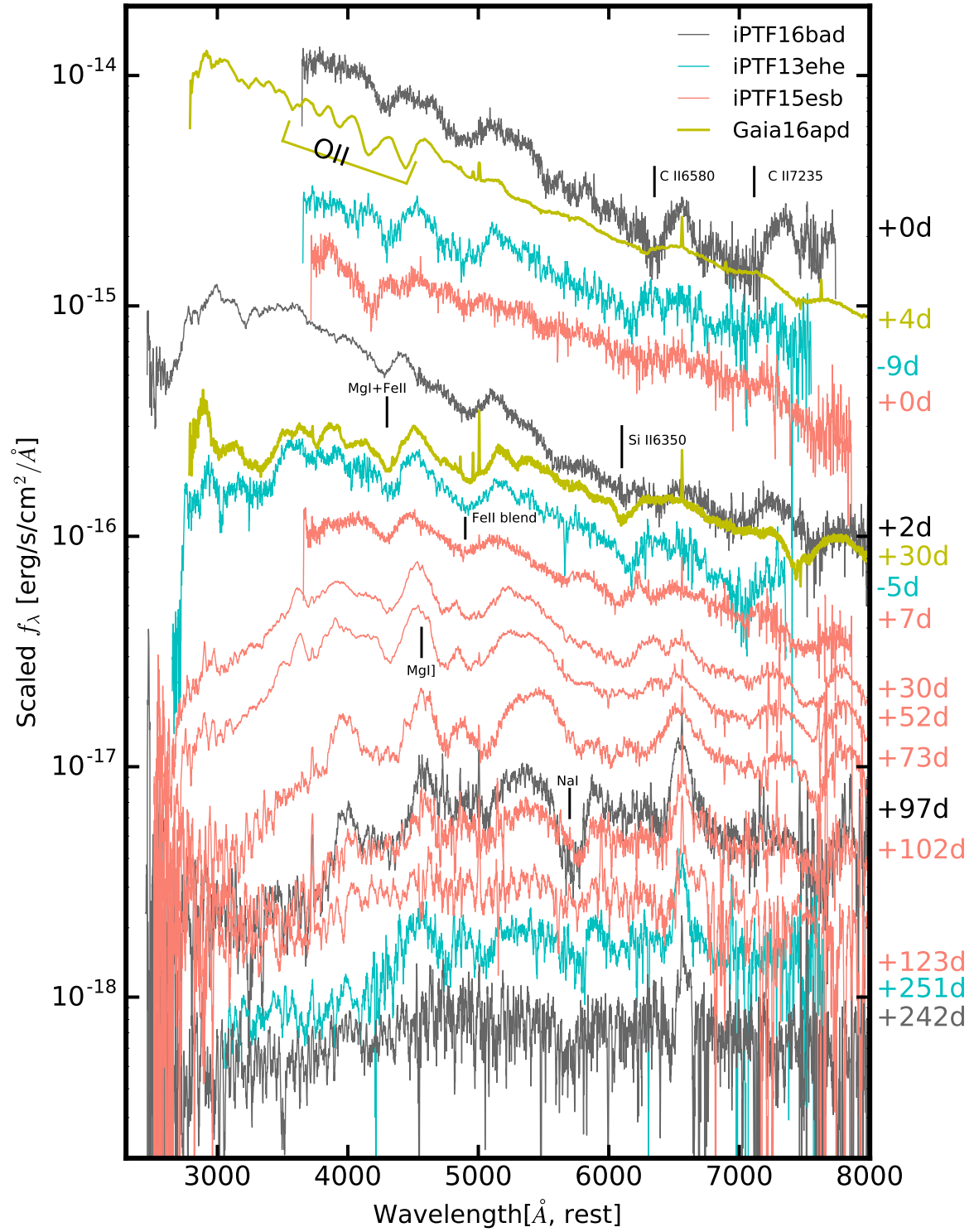


FIG. 1.— The plot displays all of the available spectra from our three SLSNe-I. We also plot the spectrum of SLSN-I Gaia16apd for comparison (Yan et al. 2016).

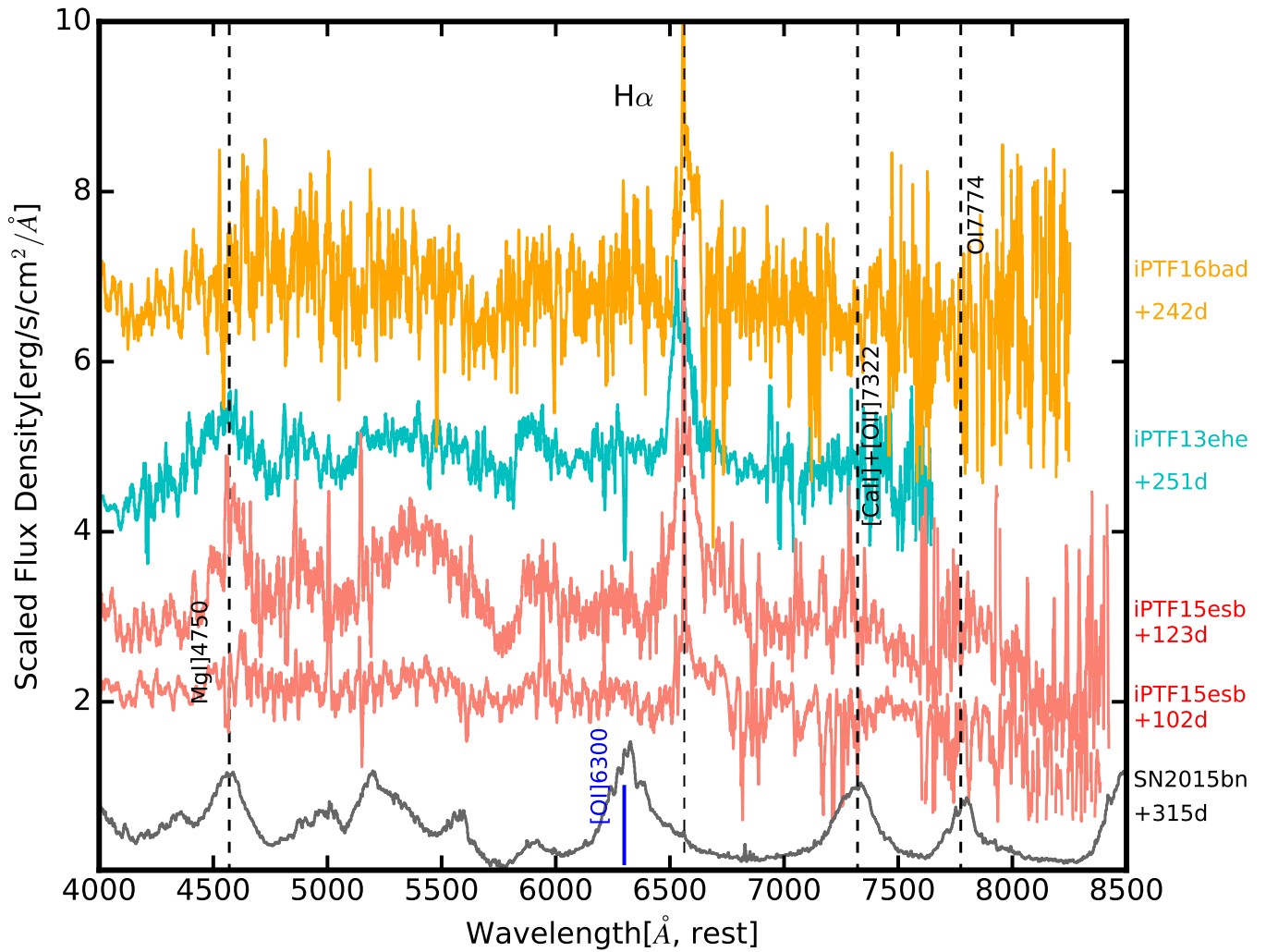


FIG. 2.— The plot displays the late time spectra of iPTF15esb, iPTF16bad, iPTF13ehe, in comparison with that of SLSN-I SN2015bn. Strong $H\alpha$ emission are detected in the spectra of the first three events.

To identify possible absorption features near the 6563Å region, we run SYNOW, the spectral synthesis code (Thomas 2013). This is a highly parametric code, including ion species, temperature, opacity, photospheric velocity, and the velocity distribution. However, it nevertheless provides a useful consistency check for line identifications. Figure 3 illustrates the two model fits to the +52 day and +0 day spectra for iPTF15esb and iPTF16bad. Clearly, the observed features near 6000 – 6700 Å can be well fit by a combination of Na I, FeII 6299, 6248Å, SiII 6347, 6371Å and CII 6580, 7234Å *absorption*, without any H α emission. This is confirmed by the actual detections of these lines at +30 day in SLSN-I Gaia16apd (Yan et al. 2016). The broad bumps around 6500Å in post-peak and pre-nebular spectra are also seen in SN2007bi and SN2015bn (Gal-Yam et al. 2009; Nicholl et al. 2016), and are considered to be a result of multiple absorption features.

By visual inspection of the available spectra, we take +73, +97 and +251 day as the first dates when H α emission lines are clearly detected. This method seems to be subjective, however, lack of full spectroscopic coverage gives much larger uncertainties in determining the true times when H α first appears.

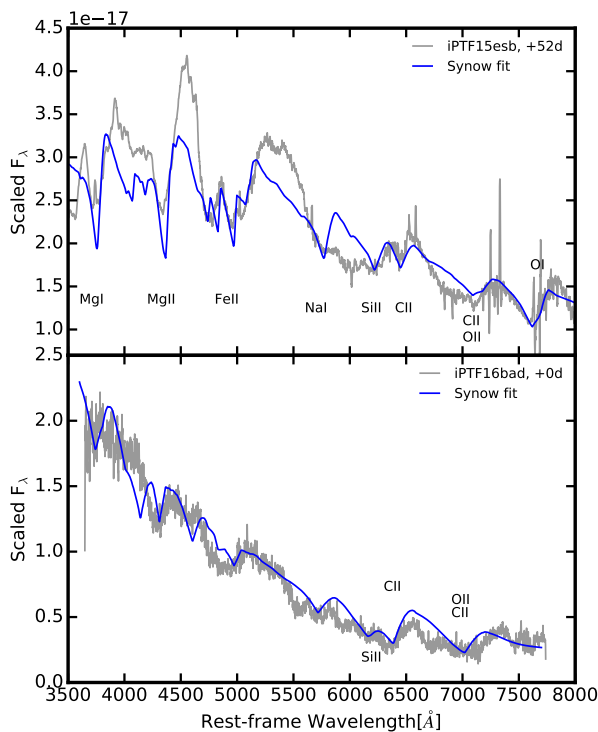


FIG. 3.— Synow model fits to the +52 day and +0 day spectra of iPTF15esb and iPTF16bad. The important wavelength region is near 6300 – 6700 Å where the H α emission is. The apparent feature at early times near 6500 Å are not due to H α emission, but produced by other broad absorptions surrounding that wavelength region.

3.2. Light Curves: Are these three SLSNe-I special?

Figure 4 presents the observed g, r, i light curves of iPTF15esb and iPTF16bad. The derived bolometric light curves are shown in Figure 5 and Figure 6. It is immediately clear that the LCs of iPTF15esb are different from a typical SLSN LC. They show semi-periodic undulations, stronger in the bluer bands and the peaks are roughly separated by ~ 22 days. Detailed discussion on the iPTF15esb LC morphology is presented in §4.3.

The peak date for iPTF15esb is chosen as the first peak at MJD = 57363.5 days. iPTF16bad has very limited photometric data. However, its r and i -band LCs in Figure 4 are initially flat, suggesting we discovered this event just before peak. Thus we set the peak date as MJD = 57540.4 days, the epoch of the first data. We construct the bolometric light curve for iPTF15esb using the following procedure. We start with a pseudo-bolometric light curve which is an integral of the broad band photometry. At each epoch with a spectrum, we calculate a bolometric luminosity using a blackbody fit. The ratio between the bolometric and pseudo-bolometric luminosity gives the bolometric correction. Without sufficient early-time photometry, we fit a power-law $L \propto t^2$ form to the pre-peak data points, and derived a minimum $t_{rise} \geq 10$ days. The late-time decay rate follows $\propto \Delta t^{-2.5}$, much steeper than the ^{56}Co decay rate (solid line). The bolometric LC for iPTF15esb is shown in Figure 5. The similar method was used for iPTF13ehe to get the bolometric light curve. iPTF16bad does not have many spectra. We derive its bolometric LC by assuming similar bolometric corrections to the pseudo-bolometric LC as that of iPTF15esb.

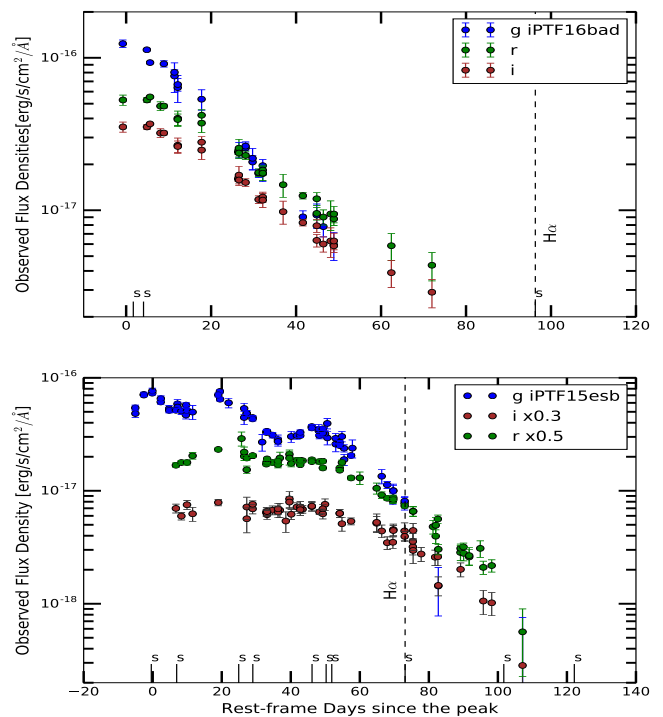


FIG. 4.— This figure presents the monochromatic light curves for g, r, i bands. The Y-axis is observed flux densities in $\text{erg}/\text{sec}/\text{cm}^2/\text{\AA}$. The first peak is at MJD=57363.5 day. The black vertical lines at the bottom of the figure mark the dates of spectroscopic observations. The dashed line indicates the date when the H α emission feature starts to appear.

One important question is: are these three SLSNe-I with late-time H α emission special and have distinctly different photometric properties compared to other SLSNe-I? The answer is relevant to understanding the nature of these events. Figure 6 makes comparison of these three LCs with other events.

iPTF15esb and iPTF16bad have peak bolometric luminosities of $\sim 4 \times 10^{43}$ erg s $^{-1}$ (-20.57 mag), whereas iPTF13ehe is more energetic, with $L_{peak} \sim 1.3 \times 10^{44}$ erg s $^{-1}$ (-21.6 mag 15). Although an unbiased SLSN-I sample does not yet exist, a simple compilation of 19 published SLSNe-I (Nicholl et al. 2015) has a median $\langle L_{peak} \rangle \sim 5.7 \times 10^{43}$ erg s $^{-1}$ (-20.7 mag).

In addition, one striking feature in Figure 6 is the large difference in evolution rates between the three LCs. For iPTF15esb and iPTF16bad, their post-peak decay rates are fast, ~ 0.05 mag/day, 3 times faster than that of iPTF13ehe, which is 0.016 mag/day. For comparison, ^{56}Co decay rate is 0.0098 mag/day. The LC evolution of iPTF15esb and iPTF16bad is similar to the fast evolving SLSN-I SN2010gx (Pastorello et al. 2010), and iPTF13ehe is more like the extremely luminous, slowly evolving SLSN-I SN2007bi (Yan et al. 2015; Gal-Yam et al. 2009). For a naive comparison with the compiled SLSN-I sample by Nicholl et al. (2015), 67% have decay rates of $0.03 - 0.05$ mag/day, and 33% of $0.01 - 0.02$ mag/day. In addition, iPTF13ehe has a rise time scale of $83 - 148$ days, implying a large ejecta mass of $70 - 220 M_{\odot}$. The other two events do not have sufficient pre-peak data, but t_{rise} in iPTF15esb is likely short, as suggested by the rising rate of the first two available observations before the peak.

We conclude that the photometric properties of these three events are clearly very different from each other. However, they are within the diverse ranges represented by the published SLSNe-I so far, with the possible exception of the unique LC morphology of iPTF15esb. Therefore, it is possible that whatever physical processes responsible for late-time H α emission could also be relevant to the whole population.

3.3. Other Spectral Properties

In the following sections, we describe other properties measured from the full spectral dataset.

3.3.1. Rapid Spectral Evolution

As shown in Figure 1, the spectra at both early and late-time are quite similar. However, they are very different from the spectra of Gaia16apd in two aspects. First, our spectra at maximum light do not have the full O II absorption series (5 features, as seen in Gaia16apd) at 4000\AA , the hallmark of a typical SLSN-I at early phases (Quimby et al. 2011). Instead, they have an absorption feature at 4200\AA which could be one of the O II absorption series. As pointed out by Mazzali et al. (2016), O II absorptions arise from highly excited O $^{+}$ with an excitation potential of ~ 25 eV. This requires collisional excitation from high temperature and density gas. At face value, our observed spectral difference could imply that near maximum light, the ejecta of these three SLSNe-I are less dense or cooler.

¹⁵ Here we assume a solar bolometric magnitude of 4.74.

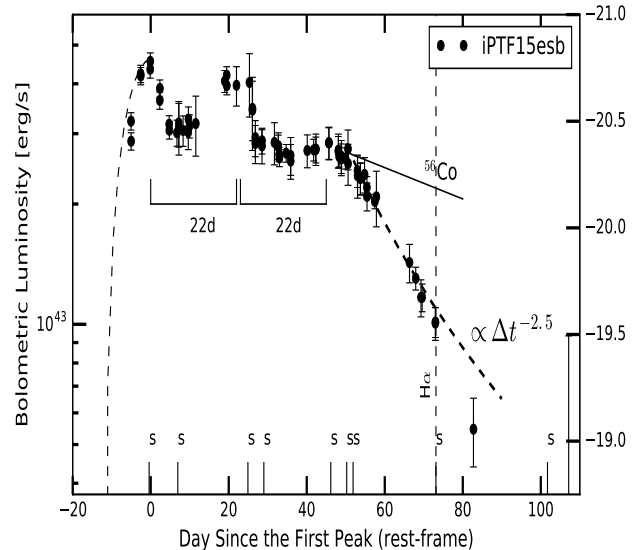


FIG. 5.— The derived bolometric light curve for iPTF15esb. Semi-periodic undulations are marked with roughly 22 days separation. The very late decay rate is $\propto t^{-2.5}$ (dashed line), steeper than the ^{56}Co rate (solid line). The vertical bars with *s* at the bottom mark the dates with spectroscopic observations.

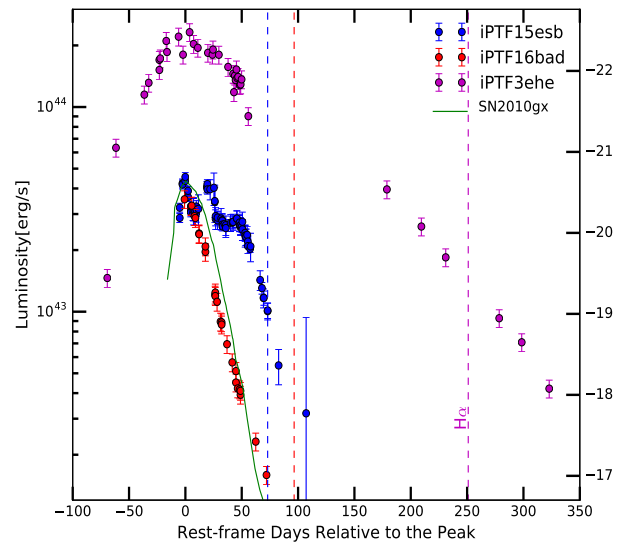


FIG. 6.— The comparison of the three bolometric light curves. The dashed vertical lines mark the dates when broad H α emission lines are detected. We also plot the bolometric LC of SLSN-I SN2010gx (green line), a SLSN-I with a fast decay rate (Pastorello et al. 2010).

The second prominent difference is that spectroscopically, iPTF13ehe and iPTF15esb seem to evolve faster than Gaia16apd, developing strong Mg I and Fe II blends at -5 and $+7$ days, characteristics of a SLSN-I at later times, such as the Gaia16apd spectrum at $+30$ day. Naively, this may seem to suggest a lower ejecta mass. This could be the case for iPTF15esb, but is not correct for iPTF13ehe at all because the slow rise time of its LC requires a very high ejecta mass (Yan et al. 2015). This suggests that spectral evolution is affected by many other

factors. The situation for iPTF16bad is not clear due to lack of sufficient spectroscopic data.

3.3.2. Higher Ejecta Velocities and Unusually High Blackbody Temperature in iPTF16bad

Figure 8 shows the ejecta velocity and the blackbody temperature as a function of time. When possible, we use FeII 5169Å, a commonly used feature, to measure the velocity evolution with time. Other FeII lines, such as FeII 4924, 5018, 5276Å are also used to cross check the results. The exception is iPTF15esb at +0 day, whose spectrum does not have a strong FeII absorption, and the ejecta velocity is estimated using O II. The O II feature in iPTF15esb is blue-shifted by 40Å relative to that of PTF09cnd at -30 day with a velocity of 15000 km s⁻¹ (Quimby et al. 2011). This implies the velocity of iPTF15esb at +0 day is roughly 17,800 km s⁻¹. The same method is applied to iPTF13ehe and iPTF16bad. We find that at maximum light, our three SLSNe-I have higher ejecta velocities than those of other published SLSNe-I, ranging between 9000 – 12000 km s⁻¹ (Nicholl et al. 2015).

The blackbody temperatures (T_{BB}) are estimated by fitting a blackbody function to the spectral continua. At maximum light, the blackbody temperatures of these three SLSNe-I range from \sim 8000 – 14000 K, with iPTF13ehe being the coolest whereas iPTF16bad the hottest. Compared with other SLSNe-I with strong O II absorption series such as PTF09cnd, SN2015bn, PTF11rks and Gaia16apd with maximum light $T_{BB} \sim$ 13000 – 15000 K (Inserra et al. 2013; Quimby et al. 2011; Nicholl et al. 2016; Yan et al. 2015), iPTF15esb and iPTF13ehe are indeed cooler at peak phase. This is consistent with their lack of the full O II absorption series discussed earlier. However, the physical reason for this lower temperature is not clear.

One of the puzzling results is the high temperatures measured from the early-time spectra of iPTF16bad because its 0 day spectrum lacks the O II absorption series, similar to that of iPTF13ehe with a lower temperature. As shown in Figure 1, the iPTF16bad early-time spectra are indeed steeper and bluer than the other two events. This difference is confirmed by their broad band ($g - r$) color versus time shown by Figure 7. We don't yet understand the physical implication of this result. It may suggest that high temperature might not be the only condition required for the formation of O II absorption series in the early-time SLSN-I spectra.

3.3.3. Broad H α Line Luminosities and Velocity Offsets

We perform simultaneous spectral fitting to the spectral continuum plus both narrow and broad H α components assuming a Gaussian profile. The narrow line fluxes are iteratively measured from the unsmoothed data. Table 5 lists the measured line luminosities and velocity widths.

One important question is whether the narrow H α line comes from the host or from the supernova. The top panel in Figure 9 shows the integrated line luminosities as a function of time. The narrow H α and [O II] lines show slight variations with time, and the changes are less than a factor of 2. In contrast, the broad H α line luminosities vary by a factor of 10 with time. Furthermore, the cen-

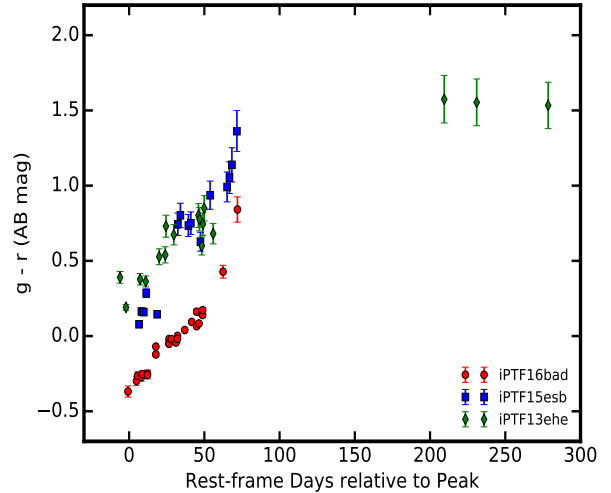


FIG. 7.— The broad-band ($g - r$) color as a function of time, showing the time evolution of the spectral slopes.

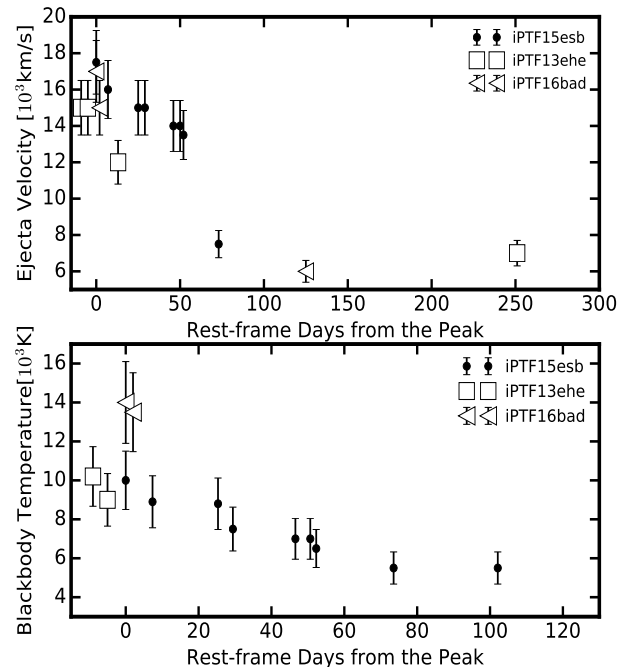


FIG. 8.— Blackbody temperature and ejecta velocity as a function of time. The velocity is measured from FeII 5169Å. The details are discussed in the text.

troids of the narrow H α emission are always at 6563Å, whereas the centroids of the broad components change with time (see below). In the case of iPTF13ehe, the spatially resolved 2-D spectrum shows that the narrow emission appears to be at the center of the host galaxy (Yan et al. 2015). We conclude that the narrow H α and [O II] emission lines are likely dominated by the host galaxies. Narrow H α emission from the supernovae may exist, but is too low luminosity to be detected by our data. The observed small variations are due to the combined effects of variable seeing and slit losses.

The middle panel in Figure 9 shows the broad $H\alpha$ line width (FWHM) as a function of time. The FWHM of $\sim 6000 - 4000 \text{ km s}^{-1}$ should not be interpreted as the shell expanding velocity. Similar to well studied SNe II powered by ejecta interaction with Circumstellar Medium (CSM), the broad line widths likely indicate the velocities of the shocked material. The H-rich CSM expansion velocity is probably much smaller, of an order of a few 100 km s^{-1} .

These three events show an interesting trend in their velocity offsets between the broad and narrow $H\alpha$ components, as shown in the bottom panel in Figure 9. We find that initially the broad components appear to be blue-shifted relative to the narrow components (assuming host emission), and at later-times, become red-shifted. The velocity offset for iPTF15esb at +73 days is as high as $+1000 \text{ km s}^{-1}$, and decreases to $\sim -400 \text{ km s}^{-1}$ at later epochs. Similarly in iPTF16bad, the offset varies from +400 to -500 km s^{-1} at +125 and 242 days. iPTF13ehe shows only positive velocity offsets (blue-shifted).

Figure 10 shows the +122 d and +242 d spectra for iPTF15esb and iPTF16bad. Although noisy, the spectra show the excess emission at the red side of $H\alpha$ 6563 Å. One possible explanation is that initially the expanding H-shell could obscure the $H\alpha$ photons from the back side which is moving away from us. So we initially see more $H\alpha$ emission from the material moving toward us (blue-shifts). In this model, at later-times when ejecta become more transparent, we should see more symmetric line profiles with no velocity offsets. This is clearly not what we see at very late-times in our data. So the red excess emission can not be explained by obscuration. We also note that the observed positive velocity offsets in all three events could be in tension with the binary model proposed by Moriya et al. (2015) for iPTF13ehe, which predicts the equal probability of observing both positive and negative velocity offsets relative to the host galaxies.

4. IMPLICATIONS AND DISCUSSIONS

4.1. Nature of the $H\alpha$ emission and implication for Helium in the ejecta

One important question is where this hydrogen material producing the late-time $H\alpha$ emission is located. One possibility is a residual hydrogen layer left over from incomplete stripping of the H-envelope. This scenario can be ruled out because if there is any hydrogen in the ejecta, it is very difficult not to have any $H\alpha$ absorption at all near maximum light, as shown in the detailed modelings carried out by Hachinger et al. (2012). This is because ejecta density is usually much higher than 10^7 cm^{-3} , and the H recombination time scale is $\propto 10^{13}/n_e$ seconds $\sim 11(n_e/10^7)^{-1}$ days, quite short. An actual example is SN 1993J, which is a type IIb SN with a very low mass of H ($< 0.9 M_\odot$). Although its pre-peak spectra have high blackbody temperatures, a weak $H\alpha$ emission is present at early phases (Filippenko et al. 1993). For our three events, at post-peak before +70 days, the photosphere temperatures are already low and there are no detectable $H\alpha$ features in all three events, even with ample spectral coverage between +0 days and +122 days for iPTF15esb.

The second possibility is a neutral, detached H-rich shell located at a distance from the progenitor star, pos-

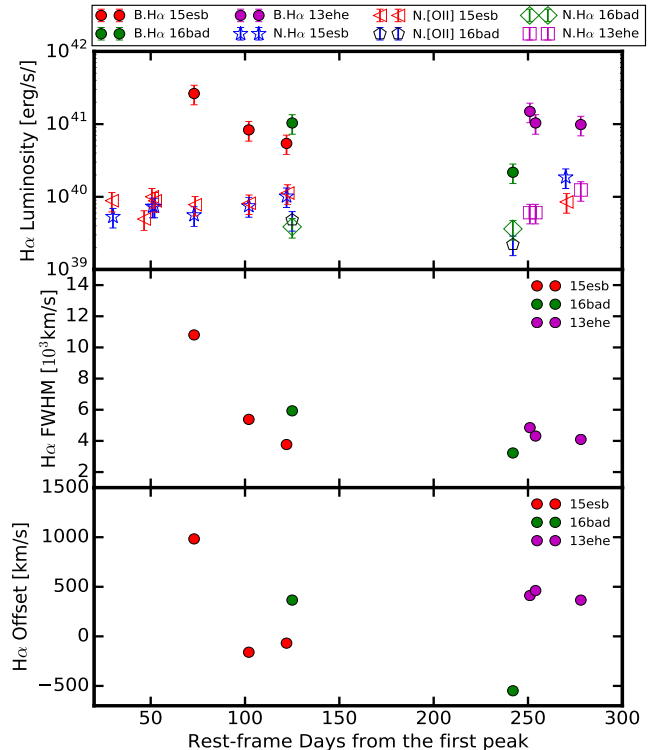


FIG. 9.— In three panels, we plot the $H\alpha$ line luminosities, line widths (FWHM) and line centroid shifts in km s^{-1} as a function of time for the three events discussed in this paper. The X-axis shows the time in days in the rest-frame, relative to the peak date for each SLSN-I.

sibly produced by a violent mass loss episode some time prior to the supernova explosion. When the ejecta eventually run into this shell, the shock interaction ionizes H atoms, and subsequent recombination produces $H\alpha$ emission. This idea was initially proposed for iPTF13ehe in Yan et al. (2015).

The third possibility is proposed by Moriya et al. (2015), where the progenitor is in a binary system with a massive, H-rich companion star ($> 20 M_\odot$). The explosive ejecta strip off a small amount of H from the companion star, which is then mixed in the inner regions of the ejecta. This H-rich material becomes visible only when the inner layers of ejecta are transparent in the nebular phases. This model predicts that depending on the orientation of the binary, there should be equal probability of seeing H-emitting material moving toward or away from us. The fact that we see blueshifts in all three events could be in tension with this prediction and disfavors this model.

Some quantitative parameters for the H-shell model can be derived from our observations. In this scenario, the progenitor is a massive star, prone to violent mass losses. Several decades before the explosion, it undergoes an eruptive episode, ejecting all of the remaining H envelope. Let us assume that the ejecta average speed is $\langle v_{ej} \rangle$ and the time between the explosion and the time $H\alpha$ is first detected is Δt . The distance traveled by the ejecta, *i.e.* the radius of this shell, is thus $R = 8.6 \times 10^{15} \left(\frac{v}{10^4 \text{ km/s}} \right) \times \left(\frac{\Delta t}{100 \text{ d}} \right) \text{ cm}$. Our measured ejecta ve-

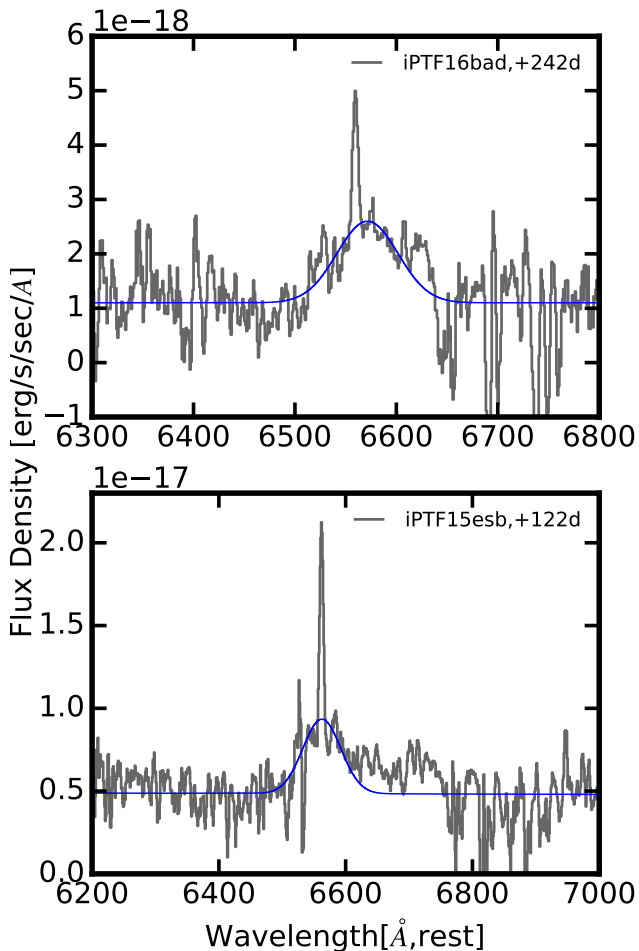


FIG. 10.— Two spectra for iPTF15esb and iPTF16bad showing some excess emission red-ward of H α 6563 Å.

locities range from 18000 – 15000 km s $^{-1}$ at maximum light to \sim 6000 – 7000 km s $^{-1}$ at +100 to +250 days. So the baseline assumption of $\langle v_{ej} \rangle \sim 10,000$ km s $^{-1}$ is not too far off.

The values of Δt are not well measured for both iPTF15esb and iPTF16bad due to poorly constrained explosion dates. For iPTF15esb, a rough estimate of Δt (Figure 4) is $73 + 20 \sim 93$ days. iPTF13ehe is a slowly evolving SLSN-I (Yan et al. 2015), with $\Delta t \sim 332$ days. Therefore, for these three events, the sizes of the H-rich shells range between $9 - 40 \times 10^{15}$ cm. If the shell expansion speed is 100 km s $^{-1}$, the time since the last episode of mass loss before explosion is $t_{erupt} \sim R/v_{shell} \sim R/100$ km s $^{-1} \sim 30$ yrs. So approximately, the last episode of mass loss is only 30 years before the supernova explosion. This time could be as short as 10 years if the expansion speed is faster. Such violent instabilities shortly before the supernova explosion could be a very common phenomenon for massive stars in general, as demonstrated for example by flash-spectroscopy of SN IIP iPTF13dqy and precursor outbursts in SNe IIn such as SN2009ip (Yaron et al. 2017; Ofek et al. 2014; Margutti et al. 2014). At lower luminosities, a similar and well studied example as our three

events is SN2014C, which was initially discovered as an ordinary SN Ib, then evolved into a strongly interacting SN IIn over ~ 1 year time scale (Milisavljevic et al. 2015; Margutti et al. 2017).

Two commonly asked questions are: (1) if this H-shell is present, why don't we see any H emission in the early-time spectra? (2) why are our spectra not being obscured or absorbed by this shell? This H-shell is likely to be neutral but optically thin during early-times. However, if spectra were taken just hours after explosion, neutral H should have been ionized and we would have detected flash spectral features (Gal-Yam et al. 2014; Yaron et al. 2017), including H α emission. For these three events, we don't detect any early-time H α emission because by the time that our first optical spectrum is taken, the H-shell has already recombined. At a density of $n \geq 10^7$ cm $^{-3}$, the H recombination time $t_{rec} \leq 10^{13}/n$ sec ≤ 11 days. For a H-shell with $R \sim 10^{16}$ cm and a width of 10% R, this density limit corresponds to a mass limit of $\geq 0.01 M_{\odot}$.

Since the H-shell is neutral at pre-peak, why don't we observe any H α absorption? H α absorption is produced when an excited H atom at $n = 2$ absorbs a photon with $\lambda = 6563$ Å, and moves up to $n = 3$ level. At temperatures of several thousands degree, most H atoms are in the ground state ($n = 1$) because the excitation energy from $n = 1$ to $n = 2$ requires 10 eV, implying a much higher temperature (10,000 K). Without excited $n = 2$ H atoms, there is no H α absorption. However, we predict that Ly α absorption ($n = 1 \rightarrow n = 2$ transition) should be strong. Future late-time UV spectroscopy may confirm this for events such as ours.

The mass of this H-shell can be constrained by two other factors. When the ejecta run into the shell, H atoms are ionized again by the thermalized kinetic energy. One constraint is that this ionized H-rich CSM can not have very high electron scattering opacity, *i.e.* Thomson scattering opacity, $\tau_{thomson} = \sigma_T n_e \Delta R \leq 1$ with ΔR being the width of the shell. Otherwise, photons from the central supernova would have been absorbed. This condition implies $M_{shell} \leq \frac{4\pi m_H R^2}{\sigma_T}$, and R is the radius of this shell. Here ΔR is cancelled out when computing the total mass. With the Thomson cross section $\sigma_T = 6.65 \times 10^{-25}$ cm 2 , we have $M_{shell} \leq 1.6 (\frac{R}{10^{16} \text{ cm}}) M_{\odot}$. Assuming the width of this shell is only 10% of the radius R , the implied electron volume density $n_e \sim 7 \times 10^9 (\frac{R}{1.0^{16} \text{ cm}}) \text{ cm}^{-3}$. The H-shell upper mass limits range from $1.6 - 30 M_{\odot}$ for the three events discussed in this paper. One scenario which could naturally explain such a powerful mass loss is the Pulsational Pair-Instability model (PPISN; Woosley et al. 2007; Woosley 2017). Further support of this model is from the weak [O I]6300 Å emission in the nebular phase spectra, as discussed below.

In the H-shell scenario, the time interval between the supernova explosion and the mass loss episode which ejected all of the H-envelope is not very long, only several decades. During this period of time, additional mass loss episodes could eject some helium layers from the progenitor star, but it is very unlikely that all of the helium can be completely removed. This implies that the ejecta of our three events may contain some Helium.

Our early spectra do not show any Helium spectral features. This might not be very surprising because the helium ionization potential is high, 24.58 eV. This would require much higher temperatures than what our spectra show, or other non-thermal ionization conditions, for example, mixing with radioactive material such as ^{56}Ni . Indeed, this condition for non-thermal ionization of He probably exist for SLSNe-I, as suggested by commonly detected five O II absorption series around 4000 Å. As argued in Mazzali et al. (2016), these O II absorption features need highly excited O^+ with an excitation potential of ~ 25 eV. The presence of O II absorption implies that the condition for producing excited O^+ should also be able to produce ionized He^+ . The puzzle is then why we do not detect any He features in our early-time spectra. We should note again that our three events are different from other SLSNe-I, and have only a partial O II absorption series in their early-time spectra.

4.2. Weak [O I] 6300 doublet emission

The [O I] 6300 doublet emission is usually very strong for SLSNe-I and SNe Ic because of the following two reasons. First, these supernovae are thought to result from the explosions of massive C+O cores. The ejecta should naturally contain a lot of oxygen. Second, the [O I] 6300 line is a very efficient coolant in the nebular phase (Jerkstrand et al. 2017). Therefore, it is common to see very strong [O I] 6300 Å emission in core collapse SNe. Figure 2 visually illustrates an apparent lack of [O I] 6300 Å emission in the late time spectra of our three events. Given the noise level in our spectra, it is not immediately clear whether this apparent discrepancy is significant, however.

To address this question, we take three late-time spectra from SLSNe-I SN2015bn at +315 and +392 day (Nicholl et al. 2016), SN2007bi at +367 day (Gal-Yam et al. 2009), which all have prominent [O I] 6300 Å emission. We scale these three spectra to the distance of iPTF16bad, *i.e.* multiply by the square of the luminosity distance ratios, and then add the noise measured from the +242 day spectrum for iPTF16bad. The simulated spectra from this procedure are shown in Figure 11. Here the noise added to the input spectra is $\sigma \sim 9 \times 10^{-19} \text{ erg s}^{-1} \text{ sec}^{-2} \text{ Å}^{-1}$, measured from the 240 Å region centered at 6300 Å (excluding H α) in the +242 day spectrum of iPTF16bad. This noise is then added as a Gaussian random noise to the input spectra. We note that because the input spectra do have their own noises, the output simulated spectra may have slightly higher RMS than the true value.

From this simple simulation, we conclude that if the +242 day spectrum from iPTF16bad were to have the same [O I] luminosity as that of the three input spectra, we would have detected this feature in our data. This implies that our spectra at $\sim +240$ days likely have intrinsically weaker [O I] 6300 Å emission than the late-time spectra of the three comparison SLSNe-I. Unfortunately, at $z \sim 0.2 - 0.3$, the Ca II triplet at 8498 Å is redshifted out of the optical range, so we do not know if the Ca II triplet is strong, and serves as an alternative cooling line for these three events. In the simulated spectra, the Ca II triplet is quite strong in SN2015bn,

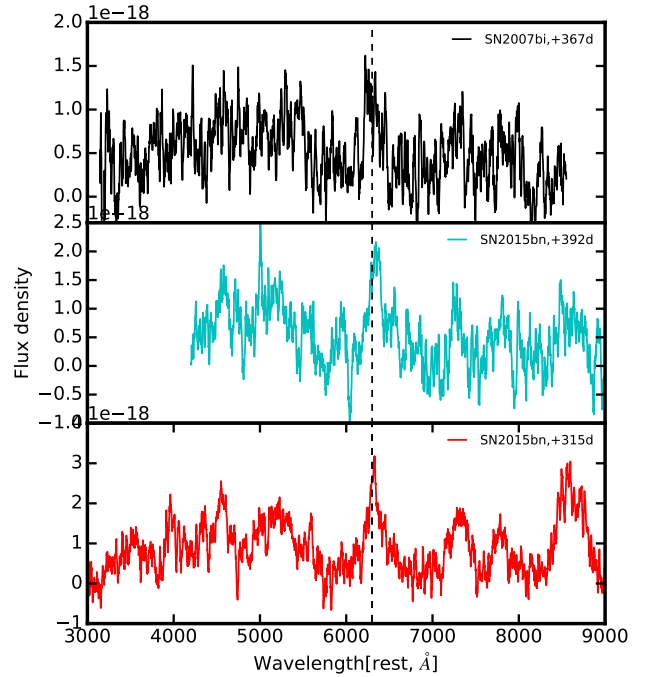


FIG. 11.— The simulated late-time spectra at the distance of iPTF16bad and with the noise of the +241 day spectrum of iPTF16bad. The input late-time spectra are from SN2007bi and SN2015bn. The dashed line marks the [O I] 6300 Å emission.

and absent in SN2007bi (see Gal-Yam et al. 2009).

The apparent weakness of the [O I] 6300 doublet and other ionized O emissions seems to suggest that there is less oxygen emitting at late-times. This is puzzling because SLSNe-I are thought to be explosive events of C+O cores with masses $>$ several tens of solar masses. There could be several explanations. First, the ejecta of our three events may have lower oxygen masses, and perhaps also lower progenitor masses than that of SN2015bn and SN2007bi. The recent modeling of the nebular spectra of SN2015bn and SN2007bi by Jerkstrand et al. (2016) has derived $M(\text{O}) \sim 10 - 30 M_{\odot}$. The second possible explanation is that these three events could be pulsational pair-instability supernova (PPISN). Calculated optical spectra at nebular phase based on pair-instability supernova (PISN) models seem to show a relatively weak [O I] 6300 doublet (Jerkstrand et al. 2016). At face value, this could be considered as supporting evidence for a PISN or PPISN model for these events. However, as shown by Jerkstrand et al. (2016), the calculated nebular spectra show very strong [Ca II] 7300 Å emission lines, which are also not detected in our late-time spectra, but are present in the simulated spectra (Figure 11). The probability of these three events being PPISN or PISN is small. First is because the required progenitor mass is very high, and secondly, as pointed by Woosley (2017), PPISN still has difficulties producing very energetic SLSNe-I, and iPTF13ehe is such an example.

The third possible explanation is that Oxygen in these three events is detached from ^{56}Ni , and with very little mixing. If the O-zone is above ^{56}Ni , γ -ray photons from ^{56}Ni decay will be effectively absorbed by Fe group

elements before reaching O. In this case, there is not sufficient photon heating to produce [O I] emission. If ejecta density is very high, it would result in high opacity, and the [O I] line may cool inefficiently. Future better modeling of nebular spectra of SLSNe-I would narrow down these possible explanations.

4.3. Nature of the LC undulations in *iPTF15esb*

What makes *iPTF15esb* stand out is its peculiar LC with strong, semi-periodic undulations, with a time scale of ~ 22 days and stronger in bluer bands. After the first peak, its *g*-band and also bolometric LC have two additional small bumps (Figure 4 & 5).

LC undulations are also seen in other SN types, such as SN2012aa (between SN Ibc and SLSN-I), other SLSNe-I (SN2015bn), SNIIn (PTF13z and SN2009ip) (Roy et al. 2016; Nicholl et al. 2016; Pastorello et al. 2013; Nyholm et al. 2017; Inserra et al. 2017). They are probably even present in SN 2007bi and PS1-14bj (Gal-Yam et al. 2009; Lunnan et al. 2016). SN2009ip is either a SNIIn or a SN imposter (Fraser et al. 2013; Graham et al. 2014; Margutti et al. 2014). Figure 12 makes a LC comparison between *iPTF15esb*, SN2012aa and SN2015bn. The LC undulation in *iPTF15esb* is quite strong, with some similarity to that of SN2012aa. These LC undulations are clearly very different from the double-peak LCs with initial weak bumps followed by prominent main peaks seen in LSQ14bdq, SN2006oz, PTF12dam and *iPTF13dcc* (Leloudas et al. 2012; Nicholl et al. 2015; Smith et al. 2016; Vreeswijk et al. 2017). Their physical nature may also be different.

Several ideas were proposed by previous studies to explain the light curves. This includes (1) successive collisions between ejecta and mass shells expelled by previous episodic mass losses; (2) magnetar UV-breakout predicted by Metzger et al. (2014); (3) recombination of certain ionized elements; (4) variable continuum optical/UV opacities which could modulate the photon diffusion, thus affecting LC morphology, as proposed for ASASSN-15lh (Godoy-Rivera et al. 2017; Margutti et al. 2017).

In the case of *iPTF15esb*, interaction based models may explain the data. The second peak has a duration of 20 days and with a net luminosity of 1.5×10^{43} erg s $^{-1}$. The total extra energy in this peak is $\sim 2 \times 10^{49}$ erg. This implies an excess luminosity of $\sim 10^{43}$ erg s $^{-1}$ over 10 days. Using a simple scaling relation $L \sim \frac{1}{2} M_{\text{csm}} v^2 / \delta t$ and taking the ejecta velocity $v_{\text{ej}} \sim 17,000$ km s $^{-1}$, we estimate $M_{\text{csm}} \sim 0.01 M_{\odot}$. Eruptive mass losses could produce such mass shells. PPISN models (Woosley 2017) could produce various successive H-poor shells, and the subsequent collisions between shells and/or ejecta-shell would generate additional energy producing the observed LC undulations.

The second possible explanation is due to the change in recombination of elements such as C and O, as shown in Piro & Morozova (2014), CSM with pure CO can undergo recombination at temperatures of roughly 8000 K. Another similar idea is the change of continuum opacity, which can naturally explain the stronger undulation in bluer bands (Godoy-Rivera et al. 2017; Margutti et al. 2017). Finally, models with central power sources, such as magnetars or fall-back accretion onto a neutron

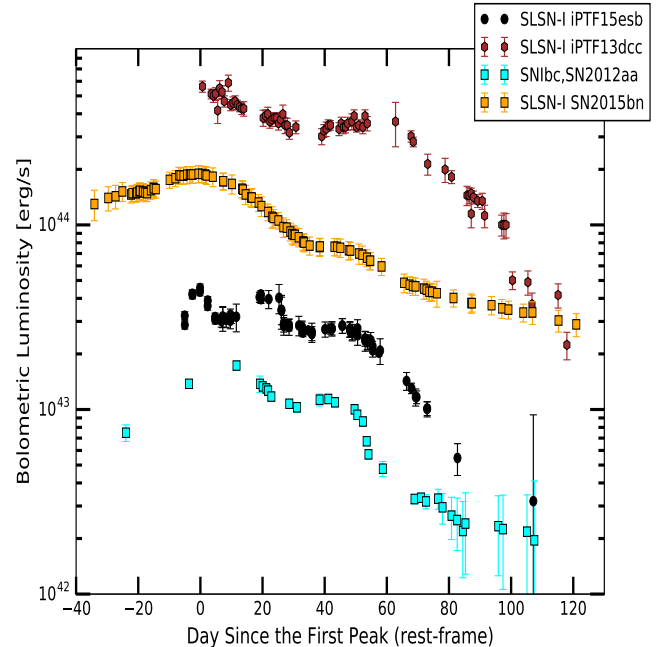


FIG. 12.— This plot compares the bolometric light curves of *iPTF15esb*, SN2012aa and SLSNe-I SN2015bn and *iPTF13dcc*. SN2012aa is a SN between SN Ibc and SLSN-I (Roy et al. 2016).

star or black hole, have an energy input function, such as $\frac{E_p}{\tau_p} \frac{1}{(1+t/\tau_p)^2}$, with E_p and τ_p as the magnetic dipole spin-down energy and the spin-down time scale respectively (Dexter & Kasen 2013; Kasen & Bildsten 2010). At late-times, the luminosity should scale like t^{-2} , close to $(t-50)^{-2.5}$, measured from the data (Figure 5). These models seem to be able to explain some data. However, the real test requires detailed calculations which can meet the challenges of all observed features.

5. SUMMARY AND CONCLUSIONS

We report two new SLSNe-I with broad H α emission in their late-time spectra discovered by *iPTF*. Together with *iPTF13ehe* (Yan et al. 2015), we now have three such events at $z \sim 0.2 - 0.3$. The H α line luminosities reach as high as $(1-3) \times 10^{41}$ erg s $^{-1}$ and the line widths range from 4000 – 10,000 km s $^{-1}$. We highlight four key observational results from our data.

First, we interpret the late-time H α emission as a result of ejecta interaction with a neutral H-shell. The shock heating ionizes the neutral H atoms, which subsequently recombine and produce H α emission. The detection of H α lines around 100–300 days since explosion imply that the H-shell must be at a distance not much farther than 10^{16} cm from the progenitor star. This shell with mass $\leq 30 M_{\odot}$ and an expansion speed of several 100 km s $^{-1}$ indicates a very energetic mass loss, which must have happened not much longer than 10 – 30 years prior to the supernova explosion. Such a tight timing provides a strong constraint on evolutionary models of massive stars.

The short time interval inferred from our H-shell model also implies that progenitor stars can not have had time to also lose all of the helium envelope. Therefore, it is likely that the ejecta of these three SLSNe-I may have some helium. The real mystery is why we do not detect

any He features in the early-time spectra, even though at early times, our three events may have sufficient non-thermal energy sources to ionize He in the ejecta, as suggested by the detections of a partial OII absorption series.

Second, the ~ 250 day spectra of two of our events show no detectable [O I] 6300 Å emission. Using simulations, we demonstrate that at these late phases, our events have intrinsically lower [O I] 6300 Å luminosities in comparison with 200 – 395 day spectra of SLSN-I SN2007bi and SN2015bn. Several different scenarios could explain this observation. The simplest one is that the ejecta of our three events may have oxygen masses less than 10 – 30 M_{\odot} , which was estimated for SN2015bn and SN2007bi (Jerkstrand et al. 2017).

The third result is that for all three events, we initially see that the broad H α lines are blue-shifted relative to the hosts. This may be in tension with the massive binary model because it predicted that we should see both red-shifted and blue-shifted H α emission lines relative to the host galaxies (Moriya et al. 2015). Interestingly, the velocity offsets between the broad H α and the host galaxies change from positive to negative with time for two of the events. The very late-time spectra (+125 and +242 days) of iPTF15esb and iPTF16bad show a weak signal of excess emission red-ward of 6563 Å. We propose that a decrease of obscuration with time could be a possible explanation for seeing through more H α emission from the back side of the H-shells.

Finally, the LC of iPTF15esb has a distinct morphology with significant undulations with a semi-periodic time scale of 22 days. Together with the evidence of H-shells, these observations paint a picture of extended and multiple CSM shells, or CSM clumps, at different radii. The LC undulation could be explained by H-poor-ejecta CSM interaction. This would require some mechanisms which can eject multiple layers of material from massive progenitor stars within a time interval of several decades before supernova explosion. One possibility is Pulsational Pair-instability supernova (Woosley 2017). Quantitative modelings of our data are needed.

With these intriguing results, one important question is how representative these three objects are among other SLSNe-I. Are they unique compared to other SLSNe-I? Photometrically, these three events are very different from each other, in their peak luminosities, and post-peak decay rates and LC morphology. However, their LC properties fall within the diverse range shown by published SLSNe-I, and are not much different from the general population of SLSN-I. Spectroscopically, these three events are very similar to each other at both early and late-times. However, they show some marked differences from other SLSNe-I, with their lack of full OII absorp-

tion series in the early-time spectra, and their higher ejecta velocities. In conclusion, our three events are not completely peculiar, but probably represent a subset of the general SLSN-I population. At face value, these three events represent (10-15)% of the PTF SLSN-I sample, although the number of events with good late-time follow-up is not large. The situation is definitely improving.

We thank N. Blagorodnova, A. Ho, Y. Cao, H. Vedantham, V. Ravi at Caltech, Melissa L. Graham, J. Mauerman, I. Shivvers and P. Kelly from University of Berkeley for taking some of the spectra for iPTF15esb. The intermediate Palomar Transient Factory project is a scientific collaboration among the California Institute of Technology, Los Alamos National Laboratory, the University of Wisconsin, Milwaukee, the Oskar Klein Center, the Weizmann Institute of Science, the TANGO Program of the University System of Taiwan, and the Kavli Institute for the Physics and Mathematics of the Universe. LNL participation in iPTF is supported by the US Department of Energy as a part of the Laboratory Directed Research and Development program. A portion of this work was carried out at the Jet Propulsion Laboratory under a Research and Technology Development Grant, under contract with the National Aeronautics and Space Administration. This paper made use of Lowell Observatory’s Discovery Channel Telescope (DCT). Lowell operates the DCT in partnership with Boston University, Northern Arizona University, the University of Maryland, and the University of Toledo. Partial support of the DCT was provided by Discovery Communications. Large Monolithic Imager (LMI) on DCT was built by Lowell Observatory using funds from the National Science Foundation (AST-1005313). This work was partially supported by the GROWTH project funded by the National Science Foundation under Grant No 1545949. This research has made use of the NASA/IPAC Extragalactic Database (NED) which is operated by the Jet Propulsion Laboratory, California Institute of Technology, under contract with the National Aeronautics and Space Administration. Some of the data presented herein were obtained at the W.M. Keck Observatory, which is operated as a scientific partnership among the California Institute of Technology, the University of California and the National Aeronautics and Space Administration. The Observatory was made possible by the generous financial support of the W.M. Keck Foundation. The authors wish to recognize and acknowledge the very significant cultural role and reverence that the summit of Mauna Kea has always had within the indigenous Hawaiian community. We are most fortunate to have the opportunity to conduct observations from this mountain.

Facilities: Palomar, Keck, Discovery Channel Telescope.

REFERENCES

- Arnett, D. 1996, *Supernovae and Nucleosynthesis: An Investigation of the History of Matter, from the Big Bang to the Present*, by D. Arnett. Princeton: Princeton University Press, 1996.,
- Benetti, S., Nicholl, M., Cappellaro, E., et al. 2014, *MNRAS*, 441, 289
- Cardelli, J. A., Clayton, G. C., & Mathis, J. S. 1989, *ApJ*, 345, 245
- Chugai, N. N. 1991, *MNRAS*, 250, 513
- Dilday, B., Howell, D. A., Cenko, S. B., et al. 2012, *Science*, 337, 942
- Dexter, J., & Kasen, D. 2013, *ApJ*, 772, 30
- Faber, S. M., Phillips, A. C., Kibrick, R. I., et al. 2003, *Proc. SPIE*, 4841, 1657
- Filippenko, A. V., Matheson, T., & Ho, L. C. 1993, *ApJ*, 415, L103

- Fox, O. D., Silverman, J. M., Filippenko, A. V., et al. 2015, *MNRAS*, 447, 772
- Fransson, C., Chevalier, R. A., Filippenko, A. V., et al. 2002, *ApJ*, 572, 350
- Fraser, M., Inserra, C., Jerkstrand, A., et al. 2013, *MNRAS*, 433, 1312
- Fremling, C., Sollerman, J., Taddia, F., et al. 2016, *A&A*, 593, A68
- Gal-Yam, A., Mazzali, P., Ofek, E. O., et al. 2009, *Nature*, 462, 624
- Gal-Yam, A. 2012, *Science*, 337, 927
- Gal-Yam, A., Arcavi, I., Ofek, E. O., et al. 2014, *Nature*, 509, 471
- Gezari, S., Halpern, J. P., Grupe, D., et al. 2009, *ApJ*, 690, 1313
- Graham, M. L., Sand, D. J., Valenti, S., et al. 2014, *ApJ*, 787, 163
- Georgy, C., Ekström, S., Meynet, G., et al. 2012, *A&A*, 542, A29
- Godoy-Rivera, D., Stanek, K. Z., Kochanek, C. S., et al. 2017, *MNRAS*, 466, 1428
- Hachinger, S., Mazzali, P. A., Taubenberger, S., et al. 2012, *MNRAS*, 422, 70
- Jerkstrand, A., Smartt, S. J., & Heger, A. 2016, *MNRAS*, 455, 3207
- Jerkstrand, A., Smartt, S. J., Inserra, C., et al. 2017, *ApJ*, 835, 13
- Kasen, D., & Bildsten, L. 2010, *ApJ*, 717, 245
- Inserra, C., Smartt, S. J., Gall, E. E. E., et al. 2016, [arXiv:1604.01226](https://arxiv.org/abs/1604.01226)
- Inserra, C., Fraser, M., Smartt, S. J., et al. 2016, *MNRAS*, 459, 2721
- Inserra, C., Smartt, S. J., Scalzo, R., et al. 2014, *MNRAS*, 437, L51
- Inserra, C., Smartt, S. J., Jerkstrand, A., et al. 2013, *ApJ*, 770, 128
- Inserra, C., Nicholl, M., Chen, T.-W., et al. 2017, [arXiv:1701.00941](https://arxiv.org/abs/1701.00941)
- Langer, N. 2012, *ARA&A*, 50, 107
- Leloudas, G., Chatzopoulos, E., Dilday, B., et al. 2012, *A&A*, 541, A129
- Leloudas, G., Schulze, S., Krühler, T., et al. 2015, *MNRAS*, 449, 917
- Lunnan, R., Chornock, R., Berger, E., et al. 2016, *ApJ*, 831, 144
- Lunnan, R., Chornock, R., Berger, E., et al. 2014, *ApJ*, 787, 138
- Nicholl, M., Berger, E., Smartt, S. J., et al. 2016, *ApJ*, 826, 39
- Nicholl, M., Smartt, S. J., Jerkstrand, A., et al. 2015, *ApJ*, 807, L18
- Nicholl, M., Smartt, S. J., Jerkstrand, A., et al. 2014, *MNRAS*, 444, 2096
- Moriya, T. J., Liu, Z.-W., Mackey, J., Chen, T.-W., & Langer, N. 2015, *A&A*, 584, L5
- Masci, F., Laher, R., Rebbapragada, U., et al. 2016, [arXiv:1608.01733](https://arxiv.org/abs/1608.01733)
- Margutti, R., Milisavljevic, D., Soderberg, A. M., et al. 2014, *ApJ*, 780, 21
- Margutti, R., Kamble, A., Milisavljevic, D., et al. 2017, *ApJ*, 835, 140
- Margutti, R., Metzger, B. D., Chornock, R., et al. 2017, *ApJ*, 836, 25
- Matheson, T., Filippenko, A. V., Ho, L. C., Barth, A. J., & Leonard, D. C. 2000, *AJ*, 120, 1499
- Mazzali, P. A., Sullivan, M., Pian, E., Greiner, J., & Kann, D. A. 2016, *MNRAS*, 458, 3455
- Metzger, B. D., Vurm, I., Hascoët, R., & Beloborodov, A. M. 2014, *MNRAS*, 437, 703
- Milisavljevic, D., Margutti, R., Kamble, A., et al. 2015, *ApJ*, 815, 120
- Miller, A. A., Chornock, R., Perley, D. A., et al. 2009, *ApJ*, 690, 1303
- Nyholm, A., Sollerman, J., Taddia, F., et al. 2017, [arXiv:1703.09679](https://arxiv.org/abs/1703.09679)
- Ofek, E. O., Cameron, P. B., Kasliwal, M. M., et al. 2007, *ApJ*, 659, L13
- Ofek, E. O., Sullivan, M., Shaviv, N. J., et al. 2014, *ApJ*, 789, 104
- Oke, J. B., & Gunn, J. E. 1982, *PASP*, 94, 586
- Oke, J. B., Cohen, J. G., Carr, M., et al. 1995, *PASP*, 107, 375
- Piro, A. L., & Morozova, V. S. 2014, *ApJ*, 792, L11
- Padmanabhan, T. 2000, *Theoretical Astrophysics - Volume 1, Astrophysical Processes*, by T. Padmanabhan, pp. 622. Cambridge University Press, December 2000. ISBN-10: 0521562406. ISBN-13: 9780521562409. LCCN: QB461 .P33 2000,
- Pastorello, A., Cappellaro, E., Inserra, C., et al. 2013, *ApJ*, 767, 1
- Pastorello, A., Smartt, S. J., Botticella, M. T., et al. 2010, *ApJ*, 724, L16
- Perley, D. A., Quimby, R. M., Yan, L., et al. 2016, *ApJ*, 830, 13
- Phinney, E. S. 1989, *The Center of the Galaxy*, 136, 543
- Planck Collaboration, Ade, P. A. R., Aghanim, N., et al. 2016, *A&A*, 594, A13
- Quimby, R. M., Kulkarni, S. R., Kasliwal, M. M., et al. 2011, *Nature*, 474, 487
- Roy, R., Sollerman, J., Silverman, J. M., et al. 2016, *A&A*, 596, A67
- Schlafly, E. F., & Finkbeiner, D. P. 2011, *ApJ*, 737, 103
- Silverman, J. M., Nugent, P. E., Gal-Yam, A., et al. 2013, *ApJ*, 772, 125
- Smith, M., Sullivan, M., D'Andrea, C. B., et al. 2016, *ApJ*, 818, L8
- Smith, N., Silverman, J. M., Chornock, R., et al. 2009, *ApJ*, 695, 1334
- Smith, N., Li, W., Foley, R. J., et al. 2007, *ApJ*, 666, 1116
- Smith, N. 2014, *ARA&A*, 52, 487
- Taddia, F., Fremling, C., Sollerman, J., et al. 2016, *A&A*, 592, A89
- Thomas, R. C. 2013, *Astrophysics Source Code Library*, [ascl:1308.008](https://arxiv.org/abs/1308.008)
- Turatto, M., Cappellaro, E., Danziger, I. J., et al. 1993, *MNRAS*, 262, 128
- Vreeswijk, P. M., Leloudas, G., Gal-Yam, A., et al. 2017, *ApJ*, 835, 58
- Woosley, S. E. 2017, *ApJ*, 836, 244
- Woosley, S. E., Blinnikov, S., & Heger, A. 2007, *Nature*, 450, 390
- Yan, L., Quimby, R., Ofek, E., et al. 2015, *ApJ*, 814, 108
- Yan, L., Quimby, R., Gal-Yam, A., et al. 2016, [arXiv:1611.02782](https://arxiv.org/abs/1611.02782)
- Yaron, O., Perley, D. A., Gal-Yam, A., et al. 2017, [arXiv:1701.02596](https://arxiv.org/abs/1701.02596)
- Yaron, O., & Gal-Yam, A. 2012, *PASP*, 124, 668

TABLE 1
THE SPECTROSCOPIC OBSERVATION LOG

Object	Obs.Date	Phase ^a days	Instrument	Exp.Time ^b seconds	Inst. Res. ^c Å
iPTF15esb	2015-12-07	+0	Keck/DEIMOS	300	4
iPTF15esb	2015-12-16	+7.4	Keck/DEIMOS	600	4
iPTF15esb	2016-01-07	+25.3	Keck/DEIMOS	600	4
iPTF15esb	2016-01-12	+29.9	Keck/LRIS	600(b),600(r)	5.6
iPTF15esb	2016-02-02	+46.5	P200/DBSP	1800	6
iPTF15esb	2016-02-07	+50.9	Keck/LRIS	1800(b),1800(r)	5.6
iPTF15esb	2016-02-09	+52.3	Keck/LRIS	1200(b), 1200(r)	5.6
iPTF15esb	2016-03-06	+73.8	Keck/LRIS	1200(b),1200(r)	5.6
iPTF15esb	2016-04-10	+102.4	Keck/LRIS	1841(b),1800(r)	5.6
iPTF15esb	2016-05-05	+122.8	Keck/LRIS	3000(b),2850(r)	5.6
iPTF15esb	2016-11-02	+270.9 ^d	Keck/LRIS	1800(b),1720(r)	5.6
iPTF15esb	2017-01-02	+320.6 ^d	Keck/LRIS	5400(b),5100(r)	5.6
iPTF16bad	2016-06-04	+2.5	Keck/DEIMOS	240	4
iPTF16bad	2016-06-07	+5.3	Keck/LRIS	240(b),240(r)	5.6
iPTF16bad	2016-09-30	+97.3	Keck/LRIS	2900(b),2700(r)	5.6
iPTF16bad	2017-03-29	+242.0	Keck/LRIS	3040(b),2800(r)	5.6

^a The rest-frame phases for iPTF15esb and iPTF16bad are relative to the peak dates of MJD = 57363.5 and 57540.4 day respectively.

^b Keck/LRIS exposure times for blue and red side can be different.

^c Instrument resolution is measured as Full-Width-Half-Maximum (FWHM) of unresolved sky lines.

^d The transient signals have mostly faded in these two spectra. They are dominated by the host galaxy light.

TABLE 2
BASIC PROPERTIES OF THE SLSNe-I IN THE SAMPLE

Name	RA J2000	DEC J2000	Redshift	$E(B - V)$ mag	u_{host} mag	g_{host} mag	r_{host} mag	i_{host} mag	z_{host} mag
iPTF13ehe	06:53:21.50	+67:07:56.0	0.3434	0.04	... ^a	24.9	24.24
iPTF15esb	07:58:50.67	+66:07:39.1	0.224	0.04	23.65	22.61	21.90	21.50	21.44
iPTF16bad	17:16:39.73	+28:22:12.6	0.2467	0.04	no-det ^b	no-det	no-det	no-det	no-det

^a iPTF13ehe is not within the SDSS foot print. Here ... means we did not obtain the host galaxy photometry in that band.

^b iPTF16bad is within the SDSS foot print. Here no-det means that the host galaxy was not detected in any of the SDSS filters. It is fainter than the SDSS detection limits.

TABLE 3
PHOTOMETRY FOR IPTF15ESB

Name	Filt	MJD day	Mag mag	Err mag	Filt	MJD day	Mag mag	Err mag	Filt	MJD day	Mag mag	Err mag
05	57371.732	20.05	0.06	r	57371.733	19.90	0.06	i	57371.734	19.83	0.07	
05	57373.663	20.07	0.08	r	57373.664	19.84	0.05	i	57373.665	20.00	0.06	
05	57375.658	20.06	0.06	r	57375.659	19.84	0.06	i	57375.661	19.75	0.07	
05	57377.652	20.09	0.18	r	57377.653	19.69	0.08	i	57377.654	19.95	0.11	
05	57386.748	19.71	0.05	r	57386.749	19.55	0.04	i	57386.750	19.70	0.05	
05	57403.879	20.52	0.06	r	57403.880	19.83	0.05	i	57403.882	19.90	0.07	
05	57405.993	20.60	0.07	r	57405.995	19.84	0.06	i	57405.996	19.87	0.07	
05	57412.618	20.63	0.14	r	57408.604	19.74	0.15	i	57408.606	19.87	0.11	
05	57414.632	20.61	0.09	r	57412.619	19.86	0.08	i	57410.711	20.11	0.16	
05	57422.622	20.61	0.08	r	57414.634	19.79	0.06	i	57412.620	19.96	0.08	
05	57424.605	20.57	0.08	r	57416.650	19.80	0.04	i	57414.635	19.8	0.07	
05	57430.603	20.63	0.13	r	57422.623	19.82	0.06	i	57416.651	19.85	0.06	
05	57444.706	21.51	0.18	r	57430.604	19.84	0.06	i	57422.625	19.91	0.04	
05	57446.656	21.70	0.09	r	57444.707	20.56	0.08	i	57424.608	19.74	0.09	
05	57448.671	22.00	0.14	r	57446.657	20.63	0.06	i	57430.606	20.17	0.11	
05	57452.814	22.11	0.16	r	57448.672	20.69	0.06	i	57444.709	20.33	0.1	
05	57452.854	22.06	0.13	r	57452.846	20.80	0.05	i	57446.658	20.59	0.1	
05	57403.800	20.39	0.04	r	57464.623	21.09	0.10	i	57448.673	20.58	0.09	
05	57433.830	20.82	0.03	r	57472.637	21.83	0.18	i	57452.811	20.33	0.14	
05	57464.770	22.33	0.06	r	57472.667	21.74	0.11	i	57452.850	20.45	0.08	
05	57494.650	22.59	0.08	r	57473.711	21.71	0.10	i	57458.699	20.84	0.11	
05	57357.326	20.00	0.07	r	57473.768	21.85	0.17	i	57463.622	20.91	0.12	
05	57357.357	20.12	0.09	r	57475.723	21.93	0.19	i	57464.6258	20.9	0.13	
05	57360.337	19.70	0.06	r	57475.729	21.90	0.21	i	57472.670	21.18	0.11	
05	57360.378	19.71	0.04	r	57479.655	21.74	0.20	i	57480.733	21.88	0.19	
05	57363.340	19.67	0.05	r	57480.727	22.16	0.16	i	57483.713	21.92	0.18	
05	57363.380	19.62	0.07	r	57483.707	22.12	0.15	i	57403.800	19.70	0.03	
05	57366.347	19.87	0.06	r	57403.800	19.72	0.03	i	57433.830	19.85	0.03	
05	57366.387	19.79	0.07	r	57433.830	19.98	0.03	i	57464.77	20.77	0.02	
05	57369.306	20.02	0.08	r	57464.770	21.08	0.02	i	57494.65	21.32	0.04	
05	57369.343	20.05	0.06	r	57494.650	21.70	0.05	i	57396.851	19.80	0.17	
05	57372.293	19.91	0.11	r	57394.988	19.31	0.17	i	57396.855	20.06	0.19	
05	57372.329	19.98	0.13	r	57395.931	19.70	0.10	i	57398.934	19.84	0.07	
05	57375.287	20.16	0.10	r	57395.935	19.61	0.13	i	57398.937	19.74	0.05	
05	57375.327	19.94	0.06	r	57396.844	20.0	0.09	i	57404.0468	19.97	0.06	
05	57387.335	19.63	0.04	r	57396.847	19.74	0.06	i	57404.0493	19.9	0.05	
05	57387.375	19.80	0.05	r	57398.929	19.69	0.04	i	57407.932	19.91	0.08	
05	57390.412	19.88	0.12	r	57398.932	19.69	0.04	i	57407.934	19.84	0.08	
05	57402.318	20.755	0.20	r	57404.042	19.83	0.04	i	57411.988	19.62	0.12	
05	57422.377	20.50	0.12	r	57404.044	19.76	0.03	i	57411.990	19.69	0.09	
05	57422.407	20.47	0.12	r	57407.927	19.89	0.07	i	57415.829	19.8	0.09	
05	57425.399	20.34	0.13	r	57407.930	19.81	0.05	i	57415.831	19.86	0.08	
05	57425.429	20.66	0.17	r	57411.983	19.66	0.11	i	57419.928	19.79	0.06	
05	57428.371	20.67	0.13	r	57411.985	19.74	0.16	i	57419.931	19.78	0.07	
05	57428.402	20.80	0.18	r	57415.824	19.89	0.03	i	57423.827	19.95	0.07	
05	57431.337	20.89	0.09	r	57415.826	19.79	0.03	i	57423.829	19.84	0.07	
05	57431.368	21.14	0.14	r	57419.923	19.78	0.04	i	57429.820	19.94	0.05	
05	57434.313	20.89	0.23	r	57419.926	19.82	0.04	i	57429.823	19.94	0.05	
05	57394.483	19.88	0.20	r	57423.822	19.81	0.04	i	57436.956	11.77	0.71	
05	57395.421	19.90	0.20	r	57423.824	19.96	0.04	i	57442.913	20.16	0.11	
05	57395.426	19.87	0.16	r	57429.812	19.96	0.03	i	57442.917	20.14	0.14	
05	57396.334	20.08	0.10	r	57429.816	20.01	0.02	i	57448.823	20.3	0.08	
05	57396.339	19.99	0.09	r	57436.952	20.18	0.15	i	57448.827	20.32	0.07	
05	57398.422	20.22	0.1	r	57442.909	20.41	0.13	i	57455.749	20.68	0.10	
05	57398.426	20.13	0.07	r	57448.816	20.62	0.05	i	57455.753	20.56	0.12	
05	57403.534	20.48	0.1	r	57448.819	20.66	0.05	i	57455.838	20.32	0.11	
05	57403.538	20.5	0.09	r	57455.830	20.92	0.10	i	57455.841	20.76	0.17	
05	57407.419	20.52	0.14	r	57455.834	20.92	0.11	
05	57407.423	20.65	0.14	r	57462.894	21.26	0.15	
05	57415.316	20.44	0.09	r	57463.850	21.47	0.14	
05	57415.320	20.43	0.11	r	57463.854	21.23	0.19	
05	57419.416	20.26	0.1	
05	57419.419	20.25	0.1	
05	57423.314	20.48	0.11	
05	57423.318	20.42	0.11	
05	57429.302	20.61	0.11	
05	57429.307	20.62	0.11	
05	57448.311	21.56	0.13	

^a All magnitudes are in AB system. No extinction correction has been applied.

TABLE 4
PHOTOMETRY FOR IPTF16BAD

Name	Filt	MJD day	Mag mag	Err mag	Filt	MJD day	Mag mag	Err mag	Filt	MJD day	Mag mag	Err mag
g	57539.921	19.10	0.06	r	57539.964	19.46	0.08	i	57547.058	19.87	0.08	
g	57546.978	19.20	0.02	r	57547.021	19.46	0.04	i	57547.060	19.81	0.07	
g	57547.908	19.41	0.02	r	57547.903	19.41	0.02	i	57547.905	19.8	0.05	
g	57551.980	19.43	0.05	r	57550.961	19.56	0.07	i	57551.977	19.88	0.08	
g	57555.085	19.63	0.23	r	57551.974	19.56	0.03	i	57574.014	20.42	0.15	
g	57555.089	19.57	0.05	r	57556.050	19.76	0.12	i	57574.018	20.53	0.16	
g	57556.042	19.82	0.21	r	57556.052	19.78	0.09	i	57575.957	20.71	0.13	
g	57556.046	19.77	0.10	r	57563.049	19.84	0.14	i	57575.960	20.69	0.12	
g	57563.045	20.01	0.16	r	57563.051	19.71	0.09	i	57579.783	20.57	0.07	
g	57574.002	20.84	0.12	r	57573.779	20.31	0.04	i	57581.009	20.58	0.21	
g	57575.954	20.81	0.08	r	57574.007	20.25	0.15	i	57589.740	20.99	0.18	
g	57575.958	20.78	0.07	r	57574.011	20.33	0.06	i	57592.783	20.96	0.07	
g	57578.008	21.04	0.11	r	57575.959	20.37	0.06	i	57596.859	21.23	0.19	
g	57578.013	20.98	0.17	r	57579.781	20.65	0.06	i	57598.781	21.01	0.09	
g	57579.785	21.23	0.06	r	57580.998	20.61	0.08	i	57601.872	21.2	0.12	
g	57580.988	21.23	0.12	r	57581.001	20.66	0.11	i	57630.662	21.87	0.17	
g	57580.993	21.10	0.10	r	57586.977	20.85	0.18	
g	57592.789	21.94	0.10	r	57592.777	21.03	0.05	
g	57596.846	21.91	0.19	r	57596.851	21.32	0.1	
g	57598.787	22.10	0.15	r	57596.855	21.08	0.1	
g	57601.855	22.40	0.22	r	57598.775	21.38	0.12	
...	r	57600.920	21.33	0.23	
...	r	57601.865	21.41	0.10	
...	r	57601.869	21.33	0.13	
...	r	57618.741	21.85	0.21	
...	r	57630.659	22.17	0.22	

^a All magnitudes are in AB system. No extinction correction has been applied.

TABLE 5
SPECTRAL LINE FIT RESULTS

Name	Phase ^a day	[OII] erg/s	N.H α erg/s	B.H α erg/s	V_{FWHM} km/s	ΔV km/s
15esb	30	8.8e+39	5.3e+39
15esb	50	4.9e+39	7.4e+39
15esb	52	1.0e+40	7.4e+39
15esb	73	8.9e+39	5.6e+39	2.6e+41	10800	1051
15esb	102	1.0e+40	7.5e+39	8.4e+40	5382	-160
15esb	122	8.1e+39	1.0e+39	5.4e+40	3768	-69
15esb	270	1.6e+40	8.5e+39
16bad	125	4.8e+39	3.9e+39	1.0e+41	5930	366
16bad	242	2.2e+39	3.6e+39	2.2e+40	3225	-549
13ehe	+251	...	6.1e+39	1.5e+41	4852	457
13ehe	+254	...	6.2e+39	1.04e+41	4312	457
13ehe	+278	...	1.24e+40	9.9e+40	4096	366

^a The rest-frame days relative to the peak date.